

# Experimental study on propagation behavior of three-dimensional cracks influenced by intermediate principal stress

Xi Z. Sun<sup>1a</sup>, B. Shen<sup>\*1,2</sup> and Bao L. Zhang<sup>1,3b</sup>

<sup>1</sup>College of Mining and Safety Engineering, Shandong University of Science and Technology, 579 Qianwangang Road, Huangdao District, Qingdao, Shandong Province, 266590, China

<sup>2</sup>Commonwealth Scientific and Industrial Research Organization (CSIRO) Energy, P.O. Box 883, Kenmore, Brisbane QLD 4069, Australia

<sup>3</sup>School of Architecture and Civil Engineering, Liaocheng University, NO.1 Hunan Road, Dongchangfu District, Liaocheng, Shandong Province, 252059, China

(Received November 20, 2016, Revised July 4, 2017, Accepted July 11, 2017)

**Abstract.** Many laboratory experiments on crack propagation under uniaxial loading and biaxial loading have been conducted in the past using transparent materials such as resin, polymethyl methacrylate (PMMA), etc. However, propagation behaviors of three-dimensional (3D) cracks in rock or rock-like materials under tri-axial loading are often considerably different. In this study, a series of true tri-axial loading tests on the rock-like material with two semi-ellipse pre-existing cracks were performed in laboratory to investigate the acoustic emission (AE) characteristics and propagation characteristics of 3D crack groups influenced by intermediate principal stress. Compared with previous experiments under uniaxial loading and biaxial loading, the tests under true tri-axial loading showed that shear cracks, anti-wing cracks and secondary cracks were the main failure mechanisms, and the initiation and propagation of tensile cracks were limited. Shear cracks propagated in the direction parallel to pre-existing crack plane. With the increase of intermediate principal stress, the critical stress of crack initiation increased gradually, and secondary shear cracks may no longer coalesce in the rock bridge. Crack aperture decreased with the increase of intermediate principal stress, and the failure is dominated by shear fracturing. There are two stages of fracture development: stable propagation stage and unstable failure stage. The AE events occurred in a zone parallel to pre-existing crack plane, and the AE zone increased gradually with the increase of intermediate principal stress, eventually forming obvious shear rupture planes. This shows that shear cracks initiated and propagated in the pre-existing crack direction, forming a shear rupture plane inside the specimens. The paths of fracturing inside the specimens were observed using the Computerized Tomography (CT) scanning and reconstruction.

**Keywords:** three-dimensional crack; true tri-axial loading; intermediate principal stress; propagation; acoustic emission; CT scan and reconstruction

## 1. Introduction

Fractured rock mass was encountered widely in geological engineering. It contained many types of original defects such as joints, fissures and fractures. The propagation of joints and fractures is a critical factor affecting the rock masses strength, and it can also induce the serious engineering incidents, such as rock burst (Wen *et al.* 2016, 2017) and water inrush (Li *et al.* 2014, 2015). Since fractured rock mass is always a three-dimensional problem in natural and it is often under the tri-axial stresses in geological engineering, it is very important to investigate the 3D crack propagation influenced by the three principal stresses.

In the past decades, experimental studies on two-

dimensional (2D) cracks propagation were carried out systematically by Shen, Reyes, Einstein, Bobet and others. (Reyes and Einstein 1991, Shen 1993, Shen *et al.* 1995, Wong and Chau 1998, Bobet and Einstein 1998, Wong and Einstein 2009a, b, Park and Bobet 2009, Janeiro and Einstein 2010, Yang 2015, Sarfarazi and Haeri 2016, Zhao *et al.* 2015). However, investigations on the 3D crack propagation are still needed to understand the true 3D fracturing processes in geological engineering.

Experimental study was the main method to understand the 3D crack propagation. Over the past few decades, several previous experiments were conducted to investigate the 3D crack propagation (Adams *et al.* 1978, Dyskin *et al.* 1999, 2003, Wong *et al.* 2004, Yang *et al.* 2010b, 2013, Wu *et al.* 1977, Jing *et al.* 2016, Majid *et al.* 2014). Most of 3D crack propagation tests were conducted under uniaxial loading, biaxial loading and conventional tri-axial loading. Few tests were conducted under true tri-axial loading condition. Due to the constraints in observation techniques, transparent materials (such as glass, PMMA) were usually used to observe the 3D crack propagation. With the influence of the material properties, the shear cracks and secondary cracks were rarely observed in these experiments (Shen 1993).

\*Corresponding author, Professor

E-mail: [baotang.shen@csiro.au](mailto:baotang.shen@csiro.au)

<sup>a</sup>Ph.D.

E-mail: [sunxizhen2008@126.com](mailto:sunxizhen2008@126.com)

<sup>b</sup>Ph.D.

E-mail: [996457633@qq.com](mailto:996457633@qq.com)

In this study, a series of true tri-axial compression tests in rock-like material were conducted on specimens containing two semi-elliptical 3D cracks. 3D crack fracturing process and propagation were observed by AE monitoring and CT scanning. The propagation behaviors and AE characteristics of 3D cracks influenced by intermediate principal stress were the main target of the investigation.

Table 1 The main mechanical parameters of the rock-like material

Mass ratio	model-gypsum: water: micro-silicon powder = 165:70:2
Unit weight	$\gamma_m=13.5 \text{ kN/m}^3$
Uniaxial compression strength	$\sigma_c=23.13 \text{ MPa}$
Uniaxial tensile strength	$\sigma_t=2.76 \text{ MPa}$
Tangent elastic modulus	$E_m=4.25 \text{ GPa}$
Cohesion	$c=3.6 \text{ MPa}$
Internal friction angle	$\varphi=31.2^\circ$

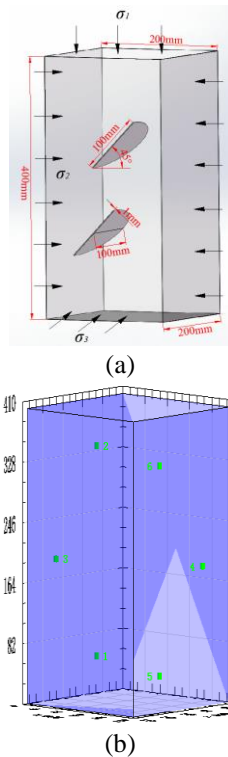


Fig. 1 3D crack configuration (a) and AE sensors layout ((b), sensor locations are described in text)

## 2. Experimental design and loading system

### 2.1 Specimen preparation

A rock-like material made of gypsum was used to conduct the tests, taken from that used by Shen (1993) for the 2D fracture propagation tests. The mechanical parameters of the rock-like material were shown in Table 1.

The size of each specimen was 200 mm wide, 200 mm long and 400 mm high. The pre-existing 3D cracks had an

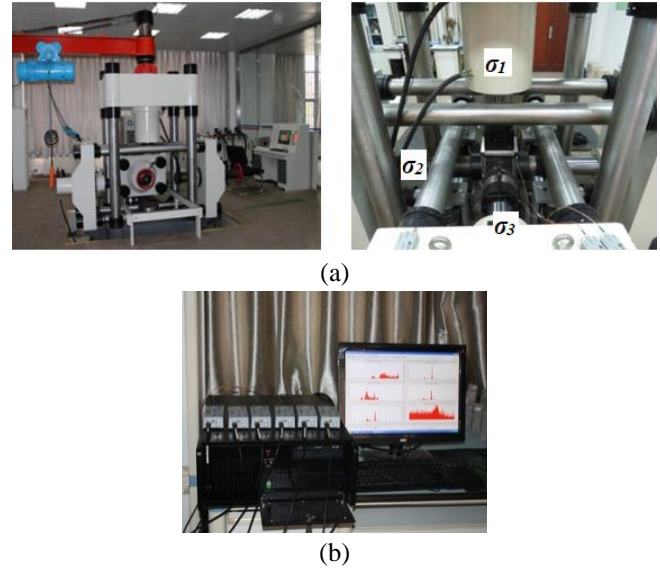


Fig. 2 The loading and monitoring system

Table 2 The AE test parameters setting

System threshold	40 dB
Floating threshold	6 dB
Sensor type	R3 $\alpha$
Resonant frequency	20-100 kHz,
Sampling frequency	$10^6/s$

inclination angle of  $45^\circ$  measured from the horizontal direction. The cracks were semi-ellipse with a minor axis length of 100 mm, a major axis length of 200 mm, and an aperture of 1 mm, as shown in Fig. 1. A total of 9 specimens were used for crack propagation testing, and they were divided into three experimental groups based on the magnitude of intermediate principal stress.

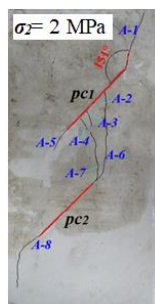
### 2.2 Testing system

A true tri-axial stress-seepage coupling rock test system (shown in Fig. 2(a)) was used to conduct the true tri-axial compression tests of specimens. This system has maximum loading stresses of  $\sigma_1=1600 \text{ kN}$ ,  $\sigma_2=1000 \text{ kN}$ ,  $\sigma_3=500 \text{ kN}$ , the max stroke of 400 mm. The measurement range of displacement sensor was 30 mm and the measuring accuracy was  $\pm 1\%$  of the measurement range. Three dimensional loading was applied through three independent servo control systems. This system allowed the true tri-axial compression tests of large-size specimens up to 200 mm wide, 200 mm long and 400 mm high.

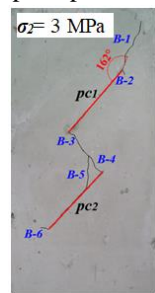
The true tri-axial compression tests of specimens were conducted in load-controlled mode at an average loading rate of 0.5 kN/s. The minor confinement stress  $\sigma_3$  was loaded to 2 MPa, and the immediate stress  $\sigma_2$  was loaded to three different levels at different tests: 2 MPa, 3 MPa, and 4 MPa. The three different levels were chosen according to the maximum deformation of specimens under three-dimensional loading and the allowable deformation of testing system. The allowable deformation of  $\sigma_1$  direction was 20 mm, and the allowable deformation of  $\sigma_2$ ,  $\sigma_3$

direction was 10 mm. According to some tentative tests, when the intermediate principal stress was equal to or greater than 5 MPa, the uniaxial deformation reached 20 mm and the specimens did not fail. Therefore, the three different levels 2 MPa, 3 MPa, and 4 MPa were chosen in this test. The major stress  $\sigma_1$  was loaded until the specimen failure. All the three stresses were loaded simultaneously at the same loading rate of 0.5 kN/s to their designed magnitudes or the peak strength of the specimen.

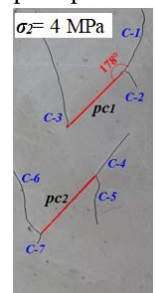
The AE characteristics of crack propagation were monitored by the PCI-2 AE System (Physical Acoustics Corporation, Princeton Jct, NJ, U.S.A.). The AE test parameters setting was shown in Table 2. The configuration of AE sensor was illustrated in Fig. 1. The six AE sensor positions were: Sensor No. 1 ( $x, y, z = 0, 50, 55$ ); Sensor No. 2 ( $0, 335, 55$ ); Sensor No. 3 ( $0, 190, 140$ ); Sensor No. 4 ( $200, 190, 55$ ); Sensor No. 5 ( $200, 50, 145$ ); and Sensor No. 6 ( $200, 335, 145$ ), the unit is mm. This configuration made it possible to monitor the whole specimen effectively, while minimizing the artificial effect of the sensor locations on the test results. Before the true tri-axial compression tests, the pencil-lead fracture method drafted by ASTM was employed to calibrate the AE system. The loading system and AE monitoring system were synchronized to have the same time stamp.



(a) Group 1-Specimen No. 1-1



(b) Group 2-Specimen No. 2-3



(c) Group 3-Specimen No. 3-3

Fig. 3 Crack propagation characteristics. *pc*-pre-existing crack

Table 3 Cracks observed in Specimen No. 1-1

Crack sequence	Initiation location	Propagation direction	Crack type
A-1	The upper tip of <i>pc</i> 1	The direction parallel to <i>pc</i> 1	Shear crack
A-2	The middle part of the <i>pc</i> 1	Vertical direction	Secondary crack
A-3	The middle part of the <i>pc</i> 1	Vertical direction	Secondary crack
A-4	The middle part of the <i>pc</i> 1	Vertical direction	Secondary crack
A-5	The lower tip of <i>pc</i> 1	The direction parallel to <i>pc</i> 1 and turned gradually towards the direction of $\sigma_1$ .	Shear crack
A-6	The upper tip of <i>pc</i> 2	The direction parallel to <i>pc</i> 2, and turned gradually towards the vertical direction.	Mixture crack
A-7	A-6	Vertical direction	Secondary crack
A-8	The lower tip of <i>pc</i> 2	The direction parallel to <i>pc</i> 2, and turned gradually towards the direction of $\sigma_1$ .	Shear crack

\**pc*-pre-existing crack,  $\sigma_1$ -the maximum principal stress. The term “shear cracks” were used for cracks initiated from the tip of pre-existing crack in the approximate direction of shear stress, and they are believed to be caused mainly by the shearing mechanism; the term “secondary cracks” were used for cracks initiated from the other parts of pre-existing crack, or from the new shear cracks, and they can be caused by both tensile and shear mechanisms depending on the propagation direction.

### 3. Propagation characteristics of 3D cracks under three-dimensional stresses

#### 3.1 Crack propagation observation

A total of nine tests in three groups (distinguished by the intermediate principal stress level) were conducted, and the typical results from each group are shown in Fig. 3.

The typical crack propagation path on the specimen surface for Specimen No. 1-1 of Group 1 was given in the Fig. 3(a) under an intermediate principal stress  $\sigma_2=2$  MPa. The details of crack geometry in Specimen No. 1-1 are listed in Table 3.

##### (1) Pre-existing crack 1 (*pc*1):

Shear crack A-1 were initiated from the tips of the *pc*1 and propagated in the direction sub-parallel to pre-existing crack. A large number of secondary cracks (A-2, A-3 and A-4) were initiated from the middle section of the *pc*1. These secondary cracks were connected with the shear crack and other secondary cracks initiated from *pc*2 in the middle part of the rock bridge. Shear crack A-5 from the lower tip propagated in the direction parallel to *pc*1 and gradually turned towards the direction of the maximum principal stress.

##### (2) Pre-existing crack 2 (*pc*2):

The propagation of shear crack A-8 was similar to shear crack A-5. Mixture crack A-6 initiated from the upper tip propagated in the direction parallel to *pc*2, and it turned gradually towards the vertical direction. The secondary crack (A-7) and mixture crack (A-6) were connected with the secondary cracks initiated from the middle section of the *pc*1 in the central part of the rock bridge.

The pre-existing cracks were compacted under three-dimensional stress condition, and the initiation and

Table 4 Cracks observed in Specimen No. 2-3

Crack sequence	Initiation location	Propagation direction	Crack type
B-1	The upper tip of $pc1$	The direction parallel to $pc1$	Shear crack
B-2	The upper tip of $pc1$	The angle of about $60^\circ$ from the $pc1$	Anti-wing crack
B-3	The lower tip of $pc1$	The angle of about $100^\circ$ from the $pc1$	Wing crack
B-4	The upper tip of $pc2$	The angle of about $90^\circ$ from the $pc2$	Wing crack
B-5	The middle part of the $pc2$	The angle of about $150^\circ$ from the $pc2$	Secondary crack
B-6	The lower tip of $pc2$	The angle of about $130^\circ$ from the $pc2$	Anti-wing crack

Table 5 Cracks observed in Specimen No. 3-3

Crack sequence	Initiation location	Propagation direction	Crack type
C-1	The upper tip of $pc1$	The direction parallel to $pc1$	Shear crack
C-2	The upper tip of $pc1$	The angle of about $90^\circ$ from the $pc1$	Anti-wing crack
C-3	The lower tip of $pc1$	The angle of about $80^\circ$ from the $pc1$	Anti-wing crack
C-4	The upper tip of $pc2$	The direction parallel to $pc2$	Shear crack
C-5	The upper tip of $pc2$	The angle of about $70^\circ$ from the $pc2$	Anti-wing crack
C-6	The lower tip of $pc2$	The angle of about $100^\circ$ from the $pc2$	Anti-wing crack
C-7	The lower tip of $pc2$	The direction parallel to $pc2$	Shear crack

propagation of tensile cracks were prohibited. The failure was dominated by shear mechanism.

The typical crack propagation path on the specimen surface of Specimen No. 2-3 of Group 2 was shown in the Fig. 3(b) under an intermediate principal stress  $\sigma_2=3$  MPa. The details of crack geometry in Specimen No. 2-3 are listed in Table 4.

(1) Pre-existing crack 1 ( $pc1$ ):

At the upper tip, a shear crack B-1 and an anti-wing crack B-2 were initiated. The shear crack B-1 propagated in the direction sub-parallel to  $pc1$ , and extended to the upper boundary of specimen. The anti-wing crack B-2 propagated at an angle of about  $60^\circ$  from the  $pc1$ , and it stopped propagating after a short distance. The wing crack B-3 initiated from the lower tip propagated at an angle of about  $100^\circ$  from the  $pc1$ .

(2) Pre-existing crack 2 ( $pc2$ ):

The wing crack B-4 and secondary crack B-5 were connected with the wing crack initiated the lower tip of  $pc1$  in the rock bridge. Micro fragmentation zones and an anti-wing crack B-6 were observed in the lower tip of  $pc2$ . The anti-wing crack B-6 stopped propagating after a short distance.

The typical crack propagation path on the specimen surface of Specimen No. 3-3 of Group 3 was shown in the Fig. 3(c) under an intermediate principal stress  $\sigma_2=4$  MPa. The details of crack geometry in Specimen No. 3-3 are listed in Table 5.

(1) Pre-existing crack 1 ( $pc1$ ):

At the upper tip, the shear crack C-1 propagated in the direction sub-parallel to  $pc1$ , and extended to the upper boundary of specimen. The anti-wing crack C-2 propagated at an angle of about  $90^\circ$  from the  $pc1$ . At the lower tip, the anti-wing crack C-3 was initiated an angle of about  $80^\circ$  from the  $pc1$ .

(2) Pre-existing crack 2 ( $pc2$ ):

Shear cracks (C-4, C-7) and anti-wing cracks (C-5, C-6) were observed. The propagation path of shear crack was short, and the anti-wing crack propagated to the left boundary of specimen.

The anti-wing cracks and shear cracks were the main crack fracture propagation types. No crack coalescence occurred in the rock bridge. The induced cracks had little aperture, the propagation mode was likely to be dominated by shear fracturing. The pre-existing cracks were compacted after specimen failure.

### 3.2 Propagation characteristics analysis

Propagation characteristics on the surface of specimens can be summarized as follows.

(1) The phenomenon of brittle-ductile transition was obvious under three-dimensional loading, and the pre-existing cracks were obviously compacted. The shear cracks, anti-wing cracks and secondary cracks were the main crack propagation types. The initiation and propagation of tensile cracks were limited. The shear cracks propagated in the direction sub-parallel to pre-existing crack.

(2) With the increase of intermediate principal stress, the number of shear cracks towards the pre-existing crack direction increased, and the initiation angle of shear crack from the upper tip of  $pc1$  also increased from  $151^\circ$  to  $178^\circ$ . The anti-wing cracks were initiated at the pre-existing crack tips. The cracks had little aperture, and the crack failure mode was shear fracturing under compression-shear condition.

## 4. Acoustic emission characteristics of 3D cracks

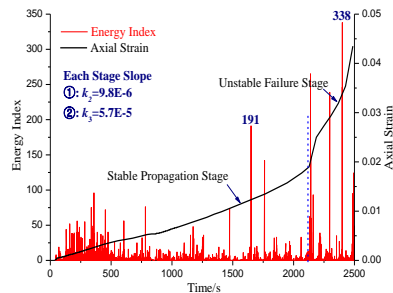
### 4.1 Acoustic emission response

For each test, the energy index, amplitude and AE event distribution were obtained from the AE monitoring and were analyzed to study the AE patterns. The relation between AE patterns and time was investigated to understand the 3D crack propagation characteristics.

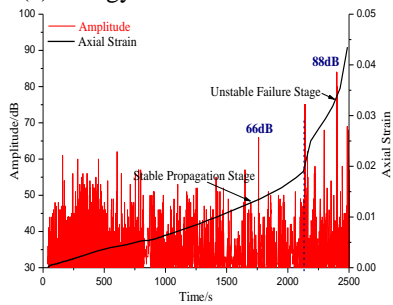
The AE signals were inevitably disturbed by test system in the true tri-axial loading process; therefore, only the channel which had been least influenced was chosen for data analysis. For large size specimens, it was difficult to locate the AE events accurately by using only six AE channels. Nevertheless, the AE event locations estimated from the monitoring system could still reflect the overall crack propagation pattern.

The AE characteristics of Specimen No. 1-1 are illustrated in Fig. 4 (Channel 1). There are two stages of fracture development based on the loading stress, i.e. stable propagation stage and unstable failure stage. In the stable stage, the cracks propagated slowly and the crack length is proportional to the increase of load. The slope of the loading curve is more or less linear, and AE event energy index remained relatively low. In the unstable stage, the cracks propagated in an accelerating manner, the AE event energy index increased sharply, the specimens eventually failed suddenly.

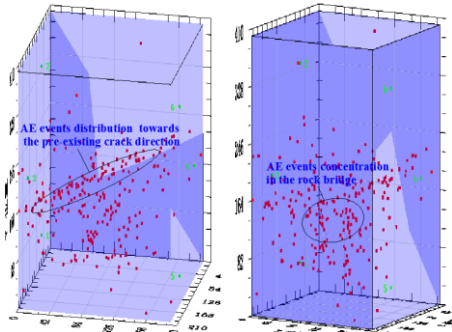
(1) Stable Propagation Stage:



(a) Energy index-time-axial strain

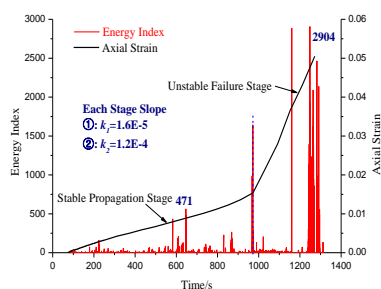


(b) Amplitude-time-axial strain

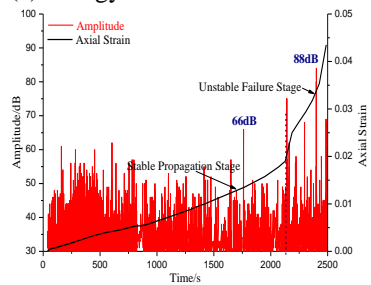


(c) AE event distribution

Fig. 4 AE characteristics of Specimen No. 1-1 (Channel 1). The energy index is defined as the envelope area of the waveform in the waveform signal. As this is an integral relationship, this parameter has no unit

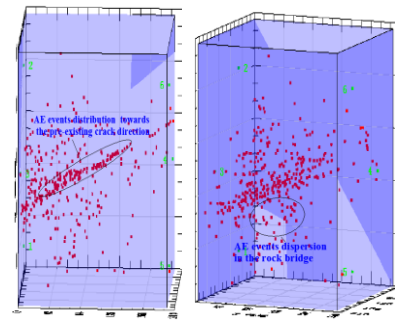


(a) Energy index-time-axial strain



(b) Amplitude-time-axial strain

Fig. 5 AE characteristics of specimen No. 2-3 (Channel 1)



(c) AE event distribution

Fig. 5 Continued

The slope of strain-time curve was  $k_1=9.8E-6$ . The maximum energy index was 191 (Fig 4(a)), and the peak amplitude was 66 dB (Fig 4(b)). The cracks propagated in the specimens, and the carrying capacity of specimens did not decrease obviously. The slope of strain-time curve kept stable, and the axial strain increased stably.

(2) Unstable Failure Stage:

The slope of strain-time curve was  $k_2=5.7E-5$ . The maximum energy index and peak amplitude were 338 and 88 dB (Fig 4(a) and 4(b)), respectively. The crack propagation led to the carrying capacity decrease. The axial strain increased sharply, and the peak frequency and strength of AE signals were much higher than that of stable propagation stage.

The AE characteristics of Specimen No. 2-3 are illustrated in Fig. 5 (Channel 1).

(1) Stable Propagation Stage:

The slope of strain-time curve was  $k_1=1.6E-5$ . The maximum energy index and peak amplitude were 471 and 85 dB, respectively (Fig. 5(a)-5(b)). The crack propagation had little influence on the carrying capacity of the specimen.

(2) Unstable Failure Stage:

The slope of strain-time curve was  $k_2=1.2E-4$ . The rate of axial strain was 7.5 times higher than that of stable propagation stage. The maximum energy index and peak amplitude were 2904 and 97 dB, respectively (Fig. 5(a) and 5(b)). The carrying capacity of specimens decreased rapidly, and the strength and frequency of AE signals were much higher than that in stable propagation stage.

The AE event distribution of Specimen No. 2-3 was shown in Fig. 5(c). The total number of AE events was 379 in the test process. The AE events clustered in the upper part of the specimen and distributed in the direction parallel to pre-existing cracks. This showed that the shear rupture occurred toward the pre-existing crack direction. The AE event density in the rock bridge was higher than that in the lower part.

The AE characteristics of Specimen No. 3-3 are illustrated in Fig. 6 (Channel 1).

(1) Stable Propagation Stage:

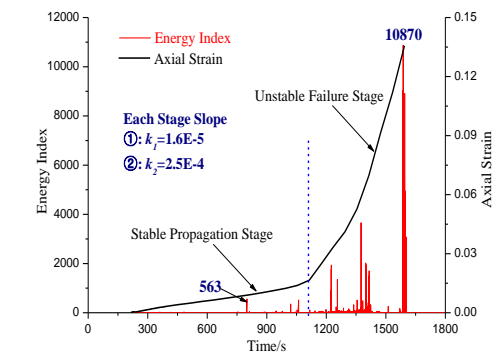
The slope of strain-time curve was  $k_1=1.6E-5$ . The maximum energy index and peak amplitude were 563 and 75 dB, respectively (Fig. 6(a) and 6(b)). The AE signal was stable and maintained at a low level. The AE signals increased gradually near the transition point between stable

propagation stage and unstable failure stage.

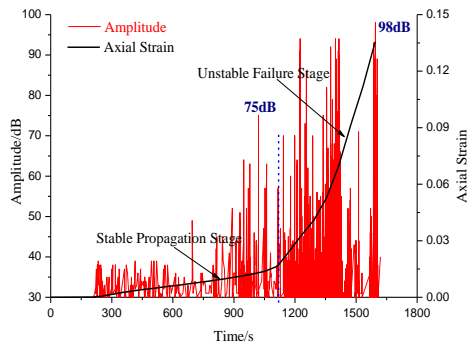
### (2) Unstable Failure Stage:

The slope of strain-time curve was  $k_2=2.5E-4$ . The maximum energy index and peak amplitude were 10870 and 98 dB, respectively (Fig 6(a) and 6(b)). The rate of axial strain was 15.6 times higher than that in stable propagation stage. Many peaks were observed with the increasing strength of amplitude. As each peak was often associated with a crack initiation or a sudden propagation, this showed that the specimen failure was induced by the multiple crack initiations and propagations.

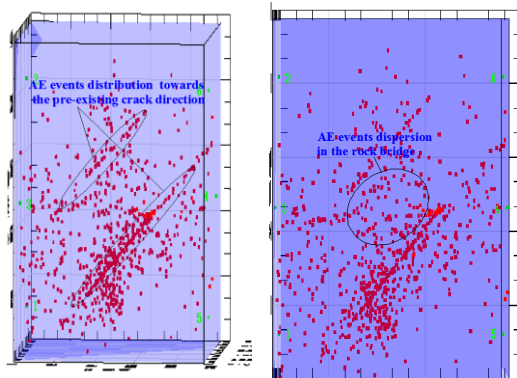
The AE event distribution of Specimen No. 3-3 was shown as Fig. 6(c). The total number of AE event was 843 during the entire test. The AE events distributed in the direction paralleled to pre-existing cracks, which implied that the shear rupture occurred toward the pre-existing crack direction. There were many AE events in the rock bridge. The AE event distribution was rather dispersed, and no cluster phenomenon appeared.



(a) Energy index-time-axial strain



(b) Amplitude-time-axial strain



(c) AE event distribution

Fig. 6 AE characteristics of Specimen No. 3-3 (Channel1)

Table 6 The characteristic parameters of AE monitoring

Specimen number	Loading stage	Strain-time curve slope	Maximum energy index	Peak amplitude/dB
No. 1-1	Stable propagation stage	$k_1=9.8E-6$	191	66
	Unstable failure stage	$k_2=5.7E-5$	338	88
No. 2-3	Stable propagation stage	$k_1=1.6E-5$	471	85
	Unstable failure stage	$k_2=1.2E-4$	2904	97
No. 3-3	Stable propagation stage	$k_1=1.6E-5$	563	75
	Unstable failure stage	$k_2=2.5E-4$	10870	98

## 4.2 Acoustic emission characteristic analysis

The characteristic parameters of AE monitoring are listed in Table 6. Acoustic emission characteristics with the increase of intermediate principal stress can be summarized as follows.

(1) There are two stages of fracture development based on the loading stress: stable propagation stage and unstable failure stage. In stable propagation stage, the axial strain was linearly increasing and AE signal strength was low. In unstable failure stage, the rate of axial strain increased rapidly, and it was 6-16 times higher than that of stable propagation stage. The AE signal strength was much higher than that in stable propagation stage.

(2) The maximum energy index in both the stable and unstable stages increased gradually with the increase of intermediate principal stress.

(3) With the increase of intermediate principal stress, the AE events tended to distribute toward the direction parallel to the pre-existing crack. This showed that the shear rupture occurred in the pre-existing crack direction, and eventually formed shear rupture planes.

## 5. 3D Crack propagation analysis

### 5.1 Computerized tomography observation

For detecting crack propagation without destruction, the Discovery CT750 HD (General Electric Company, Fairfield, CT, USA) was used to scan the 3D crack geometry after tests, as shown in Fig. 7. The scanning voltage and scanning current were 120 kV and 715 mA, respectively. The scan slice thickness and reconstruction thickness were 5 mm and 1 mm, respectively.

### 5.2 3D crack Propagation

The typical CT scanning images were shown as Fig.8. The pre-existing cracks were compacted significantly under the three-dimensional loading, and the initial aperture of  $p_c1$  disappeared completely. The shear cracks, anti-wing cracks and secondary cracks were all observed at the tips of the pre-existing cracks. A “Y” failure type was observed after termination of the pre-existing crack, and it was formed by the shear fracture zones and rock bridge failure. Shear failure was the main failure mode of the specimen under three-dimensional loading.

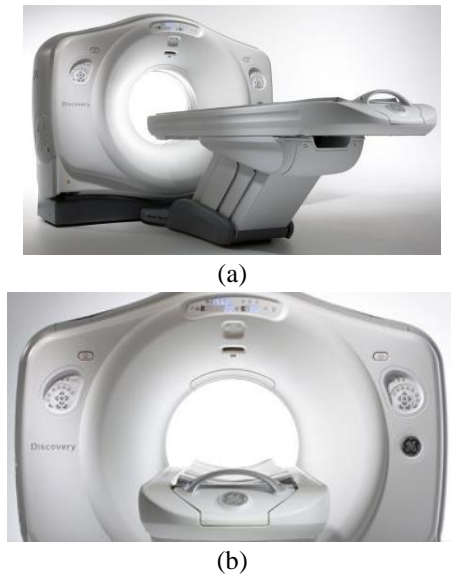


Fig. 7 Discovery CT750 HD CT System

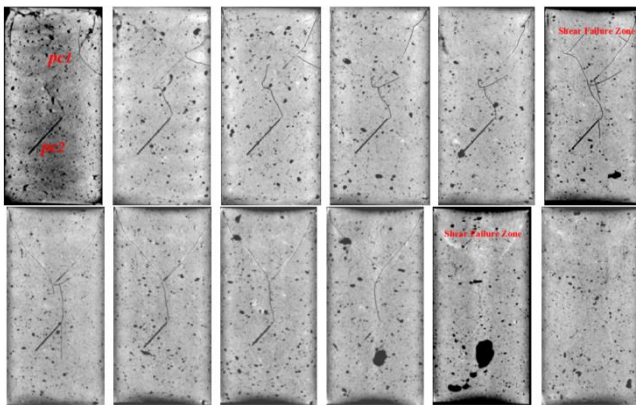


Fig. 8 Internal crack propagation of Specimen No. 1-3 at different cross-sections from one side of the specimen to the other. The 3D pre-existing cracks are gradually phased out inside the specimen. *pc*-pre-existing crack

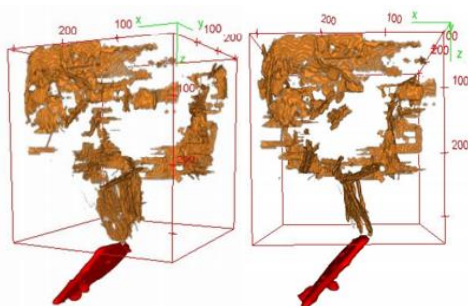


Fig. 9 3D view of crack propagation in the Specimen No. 1-3. The crack geometry was shown as Fig. 1. The red parts were the pre-existing cracks, and the yellow parts were new cracks formed in the test

The 3D crack propagation was further investigated by using CT reconstruction technique (Yun et.al, 2012). The 3D view of fractures in Specimen No. 1-3 was shown in Fig. 9.

The upper pre-existing crack was compacted too severely to be observed in the CT scan and reconstruction.

The rock bridge failure was clearly observed. Shear cracks, anti-wing cracks and secondary cracks were the main crack fracturing types. The shear cracks propagated towards the pre-existing crack direction, and the “Y” failure type was observed after the closure of the upper pre-existing crack. The failure planes appeared to be discontinuous with zig-zag geometry in the CT-scan image, which also indicated that the crack propagated as shear fracturing.

The test results were not symmetrical, and the fracturing in the upper was more severe than that in the lower part. This was believed to be caused by the loading system which had one loading end and one fixed end in each direction, and the stress attenuated gradually from the loading end to the fixed end with the influence of the friction between the specimen and the loading plates.

## 6. Conclusions

Propagation and AE characteristics of 3D cracks in rock-like material were investigated under the influence of intermediate principal stress. The main conclusions can be summarized as follows.

- Shear cracks, anti-wing cracks and secondary cracks were the main crack propagation types under three-dimensional loading. The initiation and propagation of tensile cracks were rather limited, and the fracturing was dominated by shearing under compression-shear condition.

- With the increase of intermediate principal stress, the shear cracks propagated more towards the direction parallel to the pre-existing cracks. The number of shear cracks increased gradually, and the crack aperture decreased. The failure of rock bridge could be divided into three mechanisms: pre-existing cracks coalescence with secondary cracks and shear cracks, pre-existing cracks coalescence with wing cracks, and no crack coalescence.

- There are two stages of fracture development: stable propagation stage and unstable failure stage. The maximum energy index in both the stable propagation stage and unstable failure stage increased with the increase of intermediate principal stress.

- With the increase of intermediate principal stress, AE events distributed more towards the pre-existing cracks direction, which implies that the shear rupture occurred in the same direction. By using CT scanning and reconstruction, the pre-existing cracks were found to have been compacted under three-dimensional loading. The shear cracks, anti-wing cracks and secondary cracks were observed at the tips of the pre-existing cracks. The “Y” failure type was observed after the closure of the pre-existing cracks.

## Acknowledgments

The research described in this paper was financially supported by the Natural Science Foundation of China (No. 51428401), Taishan Scholar Talent Team Support Plan for Advantaged & Unique Discipline Areas, the Natural Science Foundation of Shandong Province (No.

ZR2016EEB07), and Basic Research Project of Qingdao Source Innovation Program (No. 17-1-1-11-jch).

## References

- Adams, M. and Sines, G. (1978), "Crack extension from flaws in a brittle material subjected to compression", *Tectonophysics*, **49**(1-2), 97-118.
- Bobet, A. and Einstein, H.H. (1998), "Failure coalescence in rock-type material under uniaxial and biaxial compression", *J. Rock Mech. Min. Sci.*, **35**(7), 863-888.
- Dyskin, A.V., Germanovich, L.N. and Ustinov, K.B. (1999), "A 3-D model of wing crack growth and interaction", *Eng. Fract. Mech.*, **63**(1), 81-110.
- Dyskin, A.V., Sahouryeh, E., Jewell, R.J., Joer, H. and Ustinov, K.B. (2003), "Influence of shape and locations of initial 3-D cracks on their growth in uniaxial compression", *Eng. Fract. Mech.*, **70**(15), 2115-2136.
- Janeiro, R.P. and Einstein, H.H. (2010), "Experimental study of the cracking behavior of specimens containing inclusions (under uniaxial compression)", *J. Fract.*, **164**(1), 83-102.
- Li, L.P., Lei, T., Li, S.C., Zhang, Q.Q., Xu, Z.H., Shi, S.S. and Zhou, Z.Q. (2015), "Risk assessment of water inrush in karst tunnels and software development", *Arab. J. Geosci.*, **8**(4), 1843-1854.
- Li, L.P., Wang, Q.H., Li, S.C., Huang, H.W., Li, S.S., Wang, K., Lei, T. and Chen, D.Y. (2014), "Cause analysis of soft and hard rock tunnel collapse and information management", *Pol. J. Environ. Stud.*, **23**(4), 1227-1233.
- Majid, J.O., Mehdi, F. and Davood, T. (2014), "3-d fracture analysis of cracked aluminum plates repaired with single and double composite patches using XFEM", *Struct. Eng. Mech.*, **50**(50), 525-539.
- Park, C.H. and Bobet, A. (2009), "Crack coalescence in specimens with open and closed flaws: A comparison", *J. Rock Mech. Min. Sci.*, **46**(5), 819-829.
- Reyes, O. and Einstein, H.H. (1991), "Failure mechanism of fractured rock-a fracture coalescence model", *Proceedings of the 7th International Congress of Rock Mechanics*, Aachen, Germany, September.
- Sarfarazi, V. and Haeri, H. (2016). "A review of experimental and numerical investigations about crack propagation", *Comput. Concrete*, **18**(2), 235-266.
- Shen, B. (1993), "Mechanics of fractures and intervening bridges in hard rocks", Ph.D. Dissertation, Royal Institute of Technology, Stockholm, Sweden.
- Shen, B., Stephansson, O., Einstein, H.H. and Ghahremanli, B. (1995), "Coalescence of fractures under shear stresses in experiments", *J. Geophys. Res.*, **100**(B4), 5975-5990.
- Wang, J., Li, S.C., Zhu, W.S. and Li, L.P. (2016), "Developing brittle transparent materials with 3D fractures and experimental study", *Steel Compos. Struct.*, **22**(2), 399-409.
- Wen, Z.J., Wang, X., Tan, Y.L., Tan, Y.L. and Li, Q.H. (2016), "A study of rockburst hazard evaluation method in coal mine", *Shock Vibr.*, **2016**(16), 1-9.
- Wen, Z.J., Wang, X., Chen, L.J., Lin, G. and Zhang, H.L. (2017), "Size effect on acoustic emission characteristics of coal-rock damage evolution", *Adv. Mater. Sci. Eng.*, 1-8.
- Wong, L.N.Y. and Einstein, H.H. (2009a), "Crack coalescence in molded gypsum and carrara marble: Part 1. Macroscopic observations and interpretation", *Rock Mech. Rock Eng.*, **42**(3), 475-511.
- Wong, L.N.Y. and Einstein, H.H. (2009b), "Systematic evaluation of cracking behavior in specimens containing single flaws under uniaxial compression", *J. Rock Mech. Min. Sci.*, **46**(2), 239-249.
- Wong, R.H.C. and Chau, K.T. (1998), "Crack coalescence in a rock-like material containing two cracks", *J. Rock Mech. Min. Sci.*, **35**(2), 147-164.
- Wong, R.H.C., Huang, M.L., Jiao M.R. and Zhu, W.S. (2004), "The mechanisms of crack propagation from surface 3-D fracture under uniaxial compression", *Key Eng. Mater.*, **261-263**(I), 219-224.
- Wong, R.H.C., Law, C.M., Chau, K.T. and Zhu, W.S. (2004), "Crack propagation from 3-D surface fractures in PMMA and marble specimens under uniaxial compression", *J. Rock Mech. Min. Sci.*, **41**(S1), 219-234.
- Wu, H.C., Yao, R.F. and Yip, M.C. (1977), "Experimental investigation of the angled elliptic notch problem in tension", *J. Appl. Mech.*, **44**(3), 45-461.
- Yang, L., Jiang Y.J., Li, S.C. and Li, B. (2013), "Experimental and numerical research on 3D crack growth in rocklike material subjected to uniaxial tension", *J. Geotech. Geoenviron. Eng.*, **139**(10), 1781-1788.
- Yang, L., Jiang, Y.J., Li, S.C. and Li, B. (2010b), "Research on the propagation pattern of 3-D initial crack in rock-like material under uniaxial tension", *Key Eng. Mater.*, **452-453**(66), 817-820.
- Yang, S.Q. (2015), "An experimental study on fracture coalescence characteristics of brittle sandstone specimens combined various flaws", *Geomech. Eng.*, **8**(4), 541-557.
- Yun, T.S., Jeong, Y.J., Kim, K.Y. and Min, K.B. (2012), "Evaluation of rock anisotropy using 3D X-ray computed tomography", *Eng. Geol.*, **163**, 11-19.
- Zhao, W., Huang, R. and Yan, M. (2015), "Mechanical and fracture behavior of rock mass with parallel concentrated joints with different dip angle and number based on PFC simulation", *Geomech. Eng.*, **8**(6), 757-767.

CC